First observation by EBSD of martensitic transformations due to hydrogen presence during straining of duplex stainless steel

Claeys, L.; Depover, T.; De Graeve, I.; Verbeken, K.

Published in:
Materials Characterization

DOI:
10.1016/j.matchar.2019.109843

Publication date:
2019

First observation by EBSD of martensitic transformations due to hydrogen presence during straining of duplex stainless steel

L. Claeys[1*], T. Depover[1], I. De Graeve[1,2], K. Verbeken[1]

[1]Ghent University, Department of Materials, Textiles and Chemical Engineering, Tech Lane Ghent Science park – campus A, Technologiepark 46, 9052 Zwijnaarde, Belgium

[2]Vrije Universiteit Brussel, Department of Materials and Chemistry, Pleinlaan 2, 1050 Brussels, Belgium

*Corresponding author: Lisa.Claeys@UGent.be

Abstract

A comparative study of the active deformation mechanisms in duplex stainless steel is performed during straining with and without hydrogen charging. Interrupted tensile tests at an equal strain level clearly show that hydrogen influences how plastic deformation is accommodated. Slip planarity and martensite formation in austenite is observed for the hydrogen charged condition while dislocation multiplication and cross-slip take place for the uncharged condition. Three possibilities are put forward to explain the change: the reduction in stacking fault energy by hydrogen, a shift with respect to what phase accommodates most of the plastic strain and hydrogen pinning edge dislocations and thus restraining them to shift to the screw dislocation type and cross-slip.

Keywords: Duplex stainless steel; hydrogen; martensitic transformation; stacking fault energy; dislocation pinning

Please cite this article as: Claeys et al., First observation by EBSD of martensitic transformations due to hydrogen presence during straining of duplex stainless steel, Materials Characterisation 156 (2019) 109843, 10.1016/j.matchar.2019.109843

1. Introduction

Duplex stainless steels (DSS) are two phase materials consisting of γ-austenite (face centered cubic (FCC)) and α-ferrite (body centered cubic (BCC)). They are characterised by a combination of excellent mechanical properties and corrosion resistance. In the last decade, interest has increased in various industries, such as oil and gas, paper and chemical industry [1]. The two phase microstructure leads to a very complex deformation behaviour. Ferrite typically deforms by deformation slip due to its high amount of possible slip systems while austenite can deform by different mechanisms such as dislocation slip, twin formation and martensitic transformations depending among others on its stacking fault energy (SFE). The SFE on its turn depends on the chemical composition of the alloy and the deformation temperature [2]. For many alloying elements, the effect on the stacking fault energy is very well established. Schramm et al. [3] e.g. compared seven commercial austenitic stainless steels and concluded that Cr, Mn, Si, and N decreased the SFE while Ni and C caused an increase of the SFE. Little works include the influence of hydrogen on the stacking fault energy. In a recent paper [4], an overview is given of all available literature on the SFE in steels. The work suggested a reduction of the stacking fault energy by hydrogen. Attempts were done in determining this reduction quantitatively. Pontini et al. [5] measured a 37% reduction in AISI 304 austenitic stainless steel by XRD measurements and Robertson [6] found a 20% reduction in SFE in AISI 310 austenitic stainless steel by in-situ TEM measurements. The latter author reported that a 20% reduction will not increase the separation between partial dislocations in such a way that cross-slip will be affected for this type of austenitic stainless steel. Changes in deformation characteristics were, however, often observed under the presence of hydrogen. Ulmer et al. [7] observed strain localisation in AISI 304 and 310 stainless steel under high hydrogen concentrations. Whiteman and Troiano [8] observed a more faulted structure in an electrochemically hydrogen charged austenitic stainless steel. Nibur et al. [9] observed deformation localization in the form of slip bands in austenitic forgings. Impingements of these slip bands with each other, with twins or grain boundaries were ideal initiation sites for cracks.

Apart from slip localisation, hydrogen-induced phase transformations have been reported in austenite as well. In duplex stainless steels, transformation can be provoked by electrochemical hydrogen charging. Sobol et al. [10] showed the formation of both ε- and α'-martensite through electron backscatter diffraction (EBSD) measurements after electrochemical charging with deuterium. Glowacka et al. [11] observed the formation of α'-martensite laths in austenite through TEM measurements. The formation of martensitic phases during charging depends, however, on the severity of the applied conditions. The current density should e.g. be high enough to create large surface stresses. Hydrogen charging can also be executed without inducing phase transformations in duplex stainless steel [12], making

it possible to study the microstructural changes taking place during tensile straining. In the present work, an experimental procedure was designed to obtain a first experimental observation of the effect of hydrogen on the active deformation mechanisms during straining of charged UNS S32205 duplex stainless steel. The effect of internal hydrogen was compared with a combination of internal and external hydrogen absorbing during straining. Electron backscatter diffraction (EBSD) was used as powerful tool to study the influence of the hydrogen/material interaction on deformation and transformation [13, 14].

2. Materials and methods

The present study was performed on an as-received UNS S32205 DSS plate with a thickness of approximately 0.8 mm. The composition of the steel was according to the expectations for the grade as illustrated in Table 1. Alternating layers of austenite and ferrite were present along the rolling direction [1]. The phase fractions were more or less equal. The sample surface was prepared by standard metallographic methods including grinding and polishing. OP-U (colloidal silica, 0.04 µm) was used as final step. This resulted in a specimen thickness of 0.75 - 0.77 mm.

Table 1: Chemical composition of UNS S32205.

Wt%	C	Cr	Ni	Mo	Mn	Si	Other
UNS S32205	0.022	22.850	5.500	3.070	1.810	0.320	Cu 0.200, P 0.027, Co 0.162, N 0.173

To introduce hydrogen into the steel, electrochemical hydrogen charging was performed at a constant current density of 0.8 mA/cm² in an 0.5 M H_2SO_4 electrolyte solution containing 1 g/l thiourea to reduce the recombination to H_2. Platinum foils were used as anode. Charging was performed for 24 hours. Based on hydrogen diffusion coefficients found in literature, ranging from $2.2x10^{-14}$ m²/s to $6.4x10^{-14}$ m²/s, no homogeneous hydrogen concentration was reached through the entire thickness [15, 16, 17, 18]. This is represented schematically in Figure 1 for the $2.2x10^{-14}$ m²/s value based on the solution of the Fick's one dimensional second law for diffusion. The applied experimental methodology in this work, however, only required increased hydrogen concentrations in the near-surface region. The total hydrogen content charged into the steel with the applied conditions was measured with a Galileo G8 set-up operated with an impulse furnace and a thermal conductivity detector. Several specimens with dimensions 8x6x0.76 mm³ were melted at a temperature of 1550°C.

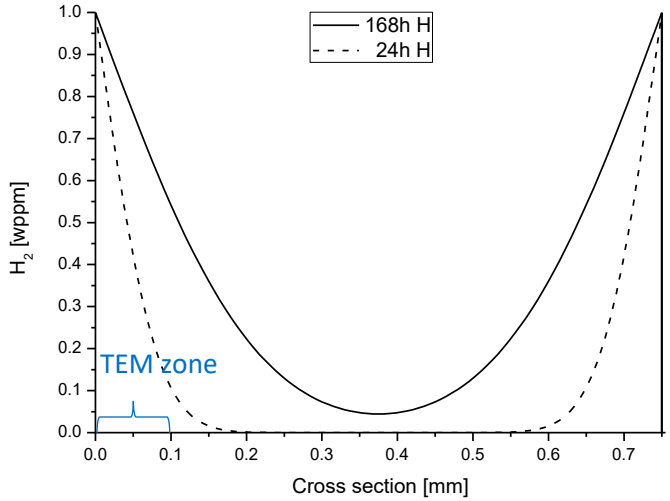

Figure 1: Normalized hydrogen distribution over the cross section of the specimen after precharging for 24 and 168 hours. The part of the specimen used as thin foil for TEM is indicated.

The mechanical behaviour of hydrogen charged and uncharged DSS was tested by means of slow strain rate tensile tests. The tensile samples were machined along the rolling direction and showed a dogbone geometry with a total length of 120 mm and a gauge section with a length of 10 mm and a width of 4 mm as illustrated in Figure 2. The rounded parts had a radius of 3 mm. The tensile tests were executed at a constant cross-head displacement speed of 0.6 mm/min, which corresponds to a strain rate of $1x10^{-3}$ s^{-1}. The uncharged tests were performed in air. These tests were compared to specimens which were hydrogen charged for 24 hours and tested either ex-situ, i.e. in air, or in-situ, i.e. with continuous hydrogen charging during the tensile test. Based on the obtained stress/strain curves, interrupted tensile tests were additionally designed to compare the active deformation mechanism in the hydrogen charged and air conditions. The tests were interrupted at 26% of engineering strain.

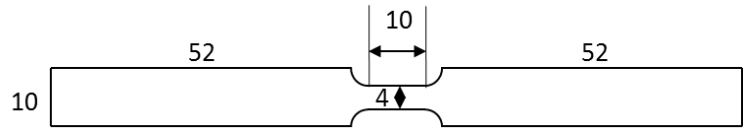

Figure 2: Tensile geometry (numbers in millimeter)

EBSD was used to study the microstructure on the normal direction (ND) plane (gauge part) of the interrupted tensile tested specimens. EBSD measurements were executed on a FEI Quanta-450 FEG scanning electron microscope (SEM) using a tilt angle of 70° and a step size of 0.07 µm for the larger scanned areas and 0.02 µm for the detailed scans both on a hexagonal grid. TSL-OIM Data analysis V7.3 software was used for post processing and analysis of the crystallographic orientation data.

TEM (JEOL JEM-2200FS) was performed to study stacking faults. For this purpose, the material was strained to 3% in order to create an adequate amount of not interacting splitted dislocations as was also done in the work of Reick et al. [19]. Both uncharged and charged specimens were strained for comparison. Charging lasted for 168 hours to have a large hydrogen affected region as indicated in Figure 1 (168 hours H). Straining of the hydrogen charged specimen was done ex-situ. The location of the thin foil created after charging and subsequent straining is indicated on Figure 1 as well. The TEM was operated with an accelerating voltage of 200 kV and a spot size of 1.5 nm.

3. Results

Figure 3 shows the engineering stress as a function of engineering strain for the uncharged and charged tests. The total hydrogen content charged into the steel after 24 hours of charging was 113.8 ± 5.8 wppm. Two tests were conducted for each condition, clearly demonstrating its reproducibility. Based on the most critical condition, i.e. the in-situ tested specimens, an engineering strain of 26% was chosen for the interrupted tests to identify the effect of hydrogen on the active deformation mechanism. These interrupted tensile tests are also included in the figure. Hydrogen charging resulted in a loss in ductility which was most pronounced for the in-situ tested specimen. Moreover, an increase in the yield strength was observed while the work hardening rate was not affected by the presence of hydrogen.

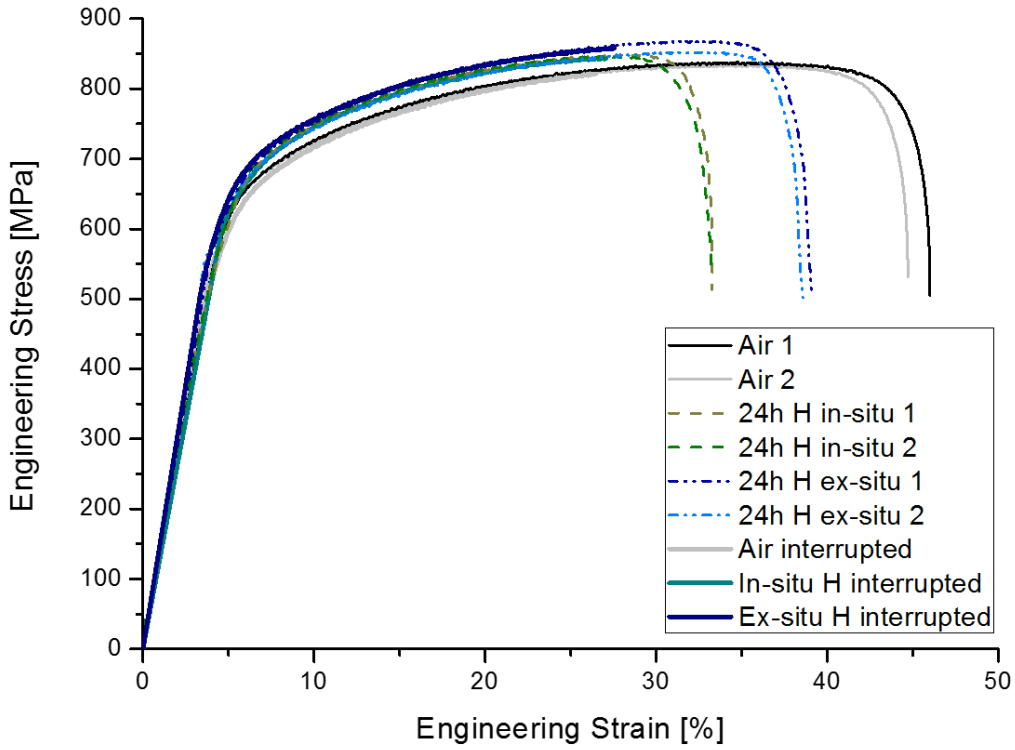

Figure 3: Engineering stress as a function of engineering strain for uncharged UNSS32205 DSS compared to 24 hours hydrogen charged and in-situ or ex-situ tensile tested specimens

Figure 4 shows the EBSD measurements on the ND surface of the interrupted tensile tests. The initial state, without hydrogen charging and deformation, is included as a reference. Both image quality maps and phase maps are shown. The difference in austenite phase fraction on the phase maps compared to the 50/50 ratio can be understood in terms of the investigated plane lying parallel to the elongated structure, which leads to either ferrite richer or austenite richer zones at the surface. Figure 5 shows a detailed EBSD measurement of a deformed austenite grain on the interrupted in-situ hydrogen charged specimen. An image quality map, inverse pole figure map and phase map are presented. Moreover, several pole figures are included of specific crystallographic directions with respect to the sample reference system. These were constructed by first creating a partition based on crystal orientation with a maximal deviation of 5°. The orientations are indicated on the inverse pole figure map. High angle grain boundaries (>15°) are indicated in black in both figures.

Clear differences can be observed in the deformation characteristics of the austenite phase. The specimen strained in air had a homogeneously increased dislocation density. In the hydrogen charged conditions, slip planarity was observed in the austenite grains. This was more pronounced in the in-situ tested specimen as indicated by the white arrows in Figure 4. Moreover, martensitic phases were additionally detected in both hydrogen charged cases. For the ex-situ tested specimen, only ε-martensite was detected. For the in-situ tested specimen, the martensitic phases consisted of both ε-martensite, the largest fraction, and α'-martensite inside the formed ε-martensite zones. Although α'-martensite is crystallographically undistinguishable from ferrite in EBSD scans, the location of a BCC phase inside the formed HCP phase, visualised in more detail in Figure 5, confirms the assumption that the α'-phase formed during deformation. In both cases, the additional martensitic transformations did not lead to an increase in work hardening. Since the transformation took place in the near-surface

region only, the martensite that formed was not able to change the macroscopic tensile behaviour.

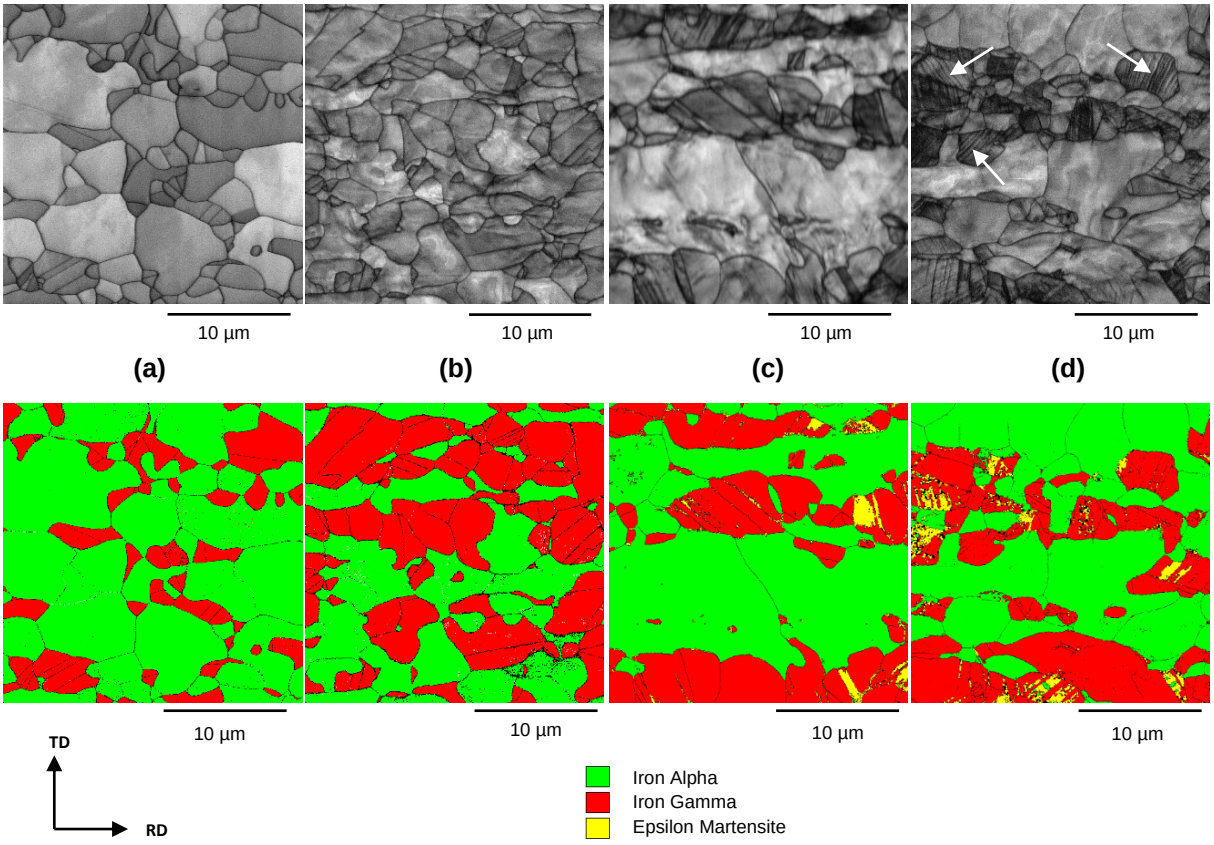

Figure 4: EBSD measurements showing image quality and phase map on (a) initial state, (b) interrupted tensile test in air, (c) ex-situ interrupted tensile test and (d) in-situ interrupted tensile test, the white arrows indicate planar slip

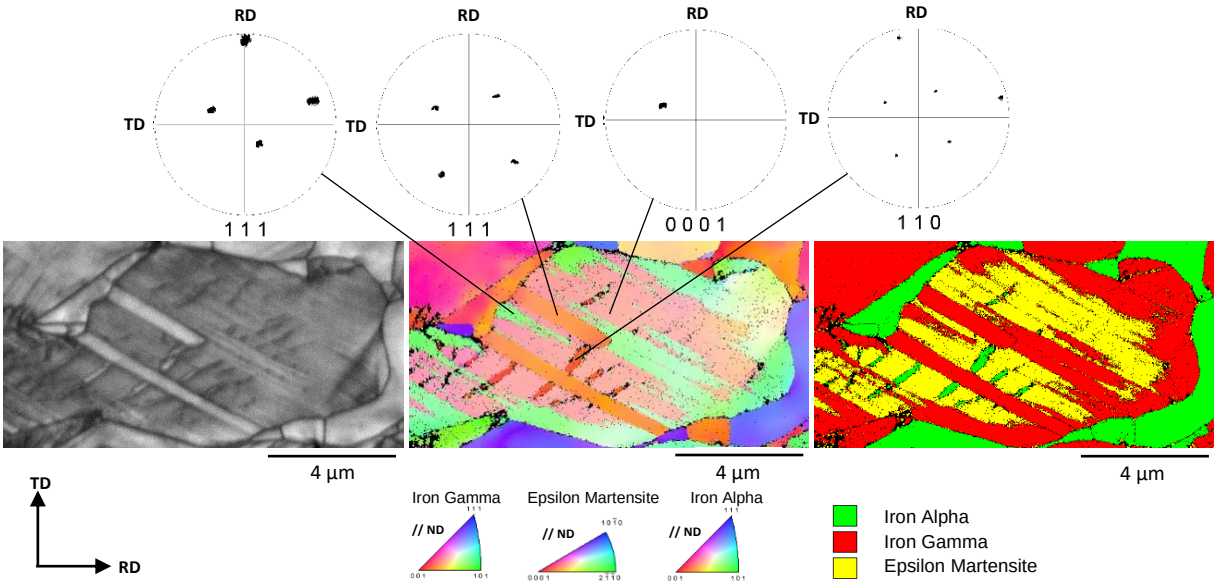

Figure 5: Detailed EBSD measurement on hydrogen charged and in-situ deformed austenite grain. Various pole figures are included.

A TEM study was performed to visualize stacking faults and subsequently relate a possible reduction in the stacking fault energy with the change in deformation mechanism. Figure 6 shows TEM images of an air strained and hydrogen charged and strained specimen. Various stacking faults were observed. Some of them are indicated by white arrows. In both cases, the stacking faults were very large and interacted with grain boundaries and/or dislocations.

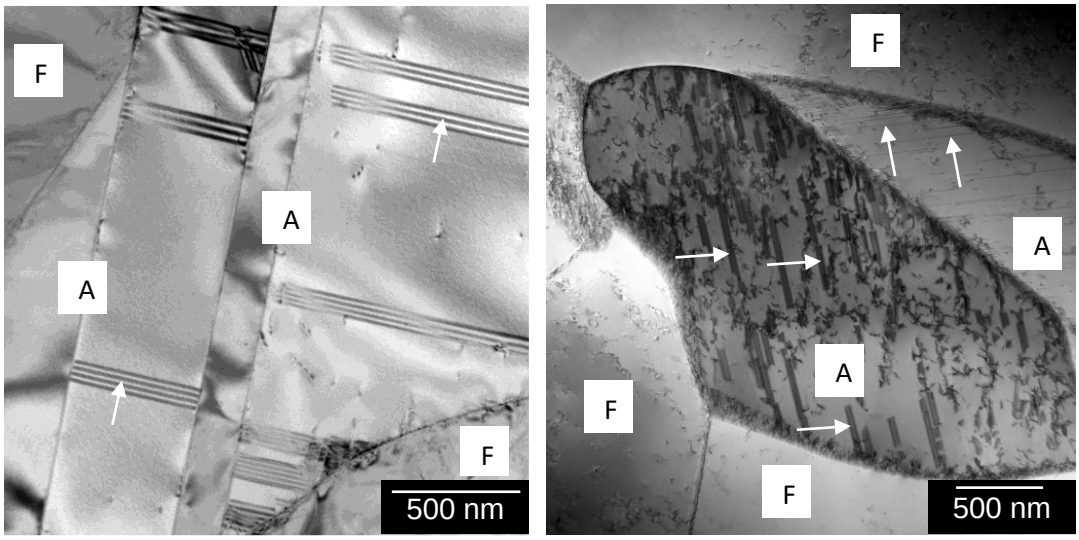

(a) **(b)**

Figure 6: TEM images of stacking faults (some of them indicated with white arrows) after straining of DSS in (a) air and (b) with hydrogen charging (ex-situ tested), A = austenite grain, F = ferrite grain

4. Discussion

Hydrogen absorbed in the microstructure of UNS S32205 had a pronounced influence on its macroscopic tensile behaviour. As expected, a distinct loss in ductility and toughness was observed when hydrogen was present [20, 21, 22]. Although hydrogen occupied only a limited region from the surface onwards as indicated in Figure 1, the effect on the tensile behaviour was significant. High surface concentrations are thus very detrimental. When hydrogen was continuously charged into the steel during straining, the ductility loss was even more pronounced. Hydrogen can in this case directly adsorb at critical locations in the steel microstructure and cause crack initiation and/or propagation. However, the increased hydrogen concentration applied during the precharging procedure is still required to observe the ductility drop since no ductility drop is present after in-situ straining without precharging. Apart from the ductility loss, hydrogen charging also increased the macroscopic yield stress. Zakroczymski et al. [20] similarly found this strengthening of DSS upon hydrogen introduction with an increasing effect for higher hydrogen concentrations. The authors did not provide an explanation for this observation. The increase might be attributed to hydrogen pinning dislocations (solid solution strengthening) [23, 24] and/or to an increased dislocation density created during charging. Concerning the latter argument, high internal stresses are present in duplex stainless steels as a result of the thermal treatment needed to create equal phase fractions at room temperature [25]. Upon introduction of hydrogen, dislocation sources start creating new dislocations due to a reduced shear modulus. Moreover, the newly emerged and already existing dislocations migrate in the steel microstructure when hydrogen is present [12, 26]. No phase transformations occurred during the charging procedure [12]. The increase in yield stress is equal for both hydrogen charged testing strategies indicating that internal hydrogen is responsible for the increase. Both proposed mechanisms can be linked to the observation. Most likely, the reason for the increased yield stress is thus a combination of both mechanisms.

Furthermore, a detailed study was executed on the potential differences on the microscopic scale via EBSD measurements. The initial state, an interrupted test in air and two interrupted tests in hydrogen charged condition (ex-situ and in-situ) were compared in Figure 4. Both slip planarity and the formation of martensitic phases can be explained by the inability of dislocations to cross-slip. As there is a general consensus that the SFE can be linked to certain microstructural deformation features in FCC alloys [4], one explanation for the change in deformation mechanism towards more planar slip is a SFE reduction by hydrogen. Stacking faults were therefore studied via TEM and were observed in large numbers both in air and hydrogen charged condition. Since stacking faults should be in equilibrium in order to measure their width accurately and correlate this width to the SFE, reliable stacking faults cannot interact

with dislocations, other stacking faults or grain boundaries. In the case of interaction with these features, the stacking faults do not develop to their equilibrium length which is determinant for the SFE [27]. The size of the stacking faults in both cases and their clear interaction with grain boundaries makes conclusions on their energy not reliable in the present alloy. Reick et al. [19] were, however, able to determine a value for the SFE of a 2205 DSS via dislocation nodes observed with TEM and found 10 mJ/m². The authors did not perform any hydrogen charging to quantify the influence of hydrogen on the stacking fault energy. They additionally concluded that although the found value is rather low, the deformation behaviour was not as expected leading to martensitic phases because ferrite mainly contributed to the deformation at high strains. This was concluded by the authors since an increasing number of austenite grains stopped participating in the deformation process at high strain values. It could therefore be argued that in the present hydrogen charged case, ferrite might be embrittled to a large extent leading to more accommodation of plastic strain by the austenite phase and hence martensitic transformations. Together with a reduction of 20-40% in SFE, as indicated in the introduction for austenitic stainless steels, this could explain the large change in observed deformation mechanism. Additionally, the inability to cross-slip can be explained by the pinning of edge dislocations by hydrogen atmospheres. Ulmer et al. [7] stated that hydrogen atoms are preferably attracted to the stress field of edge dislocations. Since a transition to the screw type is needed to cross-slip, the pinning of edge dislocations inhibits cross-slip. This hydrogen effect was already shown in aluminium where dislocation cross-slip was halted by the introduction of hydrogen visualised with TEM [28].

Ex-situ tested specimens showed the same tendency towards slip planarity and martensitic transformations as the in-situ tested specimens, however, to a lesser extent. The transformation of ε-martensite to α'-martensite e.g. did not yet proceed in the ex-situ case. All three proposed mechanisms depend on the local hydrogen concentration in the steel microstructure with higher hydrogen concentrations promoting slip planarity and martensitic transformation. During an ex-situ test, hydrogen is able to desorb, resulting in a reduced tendency to transform. During in-situ testing, on the contrary, hydrogen is additionally added to the microstructure, especially at highly stressed regions, leading to an increased tendency to transform.

Finally, a closer look was given to the mechanisms of the martensitic transformations. Crystallographic orientation with respect to the loading direction is a very important aspect for the formation of martensite. Not every austenite grain in Figure 4 has an equal tendency to form martensitic phases. The austenite grain in Figure 5 contains annealing twins with a different orientation compared to the parent grain that are free of martensite while the parent grain underwent martensite transformations. The formation of ε-martensite happens by the

gliding of Shockley partial dislocations on every second $\{111\}_\gamma$ plane [2]. The Shoji-Nishiyama orientation relationship is established between austenite and ε-martensite, i.e. $\{111\}_\gamma//\{0001\}_\varepsilon$ and $<110>_\gamma//<11\text{-}20>_\varepsilon$ [2, 29]. The former is visualised by the first and third pole figure (figure 4) in which a clear overlap of the $[0001]_\varepsilon$ pole with one of the $<111>_\gamma$ poles was observed. One single variant of ε-martensite was formed in the austenite grain in figure 4. The formation of ε-martensite is, however, an intermediate step towards the formation of α'-martensite. Yang et al. [29] elaborated on the formation of α'-martensite out of single ε-laths during the γ→ε→α' martensitic phase transformation in 304 stainless steel. It is energetically preferred to nucleate α'-martensite inside preformed ε-martensite laths rather than in the γ-matrix. However, in most cases, α'-martensite nucleates at the intersection of two ε-martensite laths and the mechanism is rather well established. Yang et al. [29] concluded that the nucleation in one ε-martensite lath follows the same mechanism. Moreover, the Kurdyumov-Sachs orientation relationship is obeyed, i.e. $\{111\}_\gamma//\{0001\}_\varepsilon//\{110\}_{\alpha'}$ and $<110>_\gamma//<11\text{-}20>_\varepsilon//<111>_{\alpha'}$ [2, 29]. The pole figures in the present case show the same trend. The $[0001]_\varepsilon$ pole can be found in all pole figures. The twin orientation relation, i.e. 60°<111>, is established by the shared pole with both martensitic phases.

It could be interesting to study the influence of the martensitic transformations on crack initiation and propagation. It is debated in literature whether martensite formation is critical in the explanation of hydrogen embrittlement occurring in austenitic steels. Various authors state that the martensitic transformation is responsible for hydrogen embrittlement [30, 31]. Martensite formation at the crack tip is also stated to aid the propagation of cracks [32]. In contradiction, other authors mentioned that martensite formation is neither necessary nor sufficient to explain the observed hydrogen embrittlement of austenitic steels [33].

5. Conclusion

Uncharged and hydrogen charged interrupted tensile tested specimens of UNS S32205 DSS were investigated to evaluate their active deformation mechanisms. Planar slip and both ε- and α'-martensite were detected in the austenite phase of the hydrogen charged specimens being more pronounced for in-situ testing compared to ex-situ tensile testing. Both phenomena were absent in the case of uncharged specimens. This could be explained by a reduction in SFE accompanied with a shift in which phase accommodates most of the plastic deformation. Also, the additional pinning of edge dislocations by hydrogen atmospheres inhibiting cross-slip contributed to the large difference in observed deformation mechanism. The austenite to martensite transformation happened in correspondence to established mechanisms.

6. Acknowledgements

The authors acknowledge Aperam Genk for the received duplex stainless steel plate. The research was also supported by FWO (SB PhD fellow project number 1S16618N) and the special research fund (BOF) of Ghent University (grant BOF01P03516 and grant BOF15/BAS/062 for the used equipment).

7. Data availability

The raw/processed data required to reproduce these findings cannot be shared at this time as the data also forms part of an ongoing study.

8. References

[1] I. Alvares-Armas and S. Degallaix-Moreuil, Duplex stainless steels, John Wiley & Sons, 2009.

[2] C. Herrera, D. Ponge and D. Raabe, “Design of a novel Mn-based 1 GPa duplex stainless TRIP steel with 60% ductility by a reduction of austenite stability,” *Acta materialia,* vol. 59, pp. 4653-4664, 2011.

[3] R. Schramm and R. Reed, “Stacking fault energy of seven commercial austenitic stainless steels,” *Metallurgical transactions A,* vol. 6, pp. 1345-1351, 1975.

[4] A. Das, “Revisiting stacking fault energies of steels,” *Metallurgical and materials transactions A,* vol. 47, no. 2, pp. 748-768, 2016.

[5] A. Pontini and J. Hermida, “X-ray diffraction measurement of the stacking fault energy reduction induced by hydrogen in an AISI 304 steel,” *Scripta materialia,* vol. 37, no. 11, pp. 1831-1837, 1997.

[6] P. Ferreira, I. Robertson and H. Birnbaum, “Influence of hydrogen on the stacking fault energy of an austenitic stainless steel,” *Materials Science Forum,* Vols. 207-209 (PART I), pp. 93-96, 1996.

[7] D. Ulmer and C. Altstetter, “Hydrogen-induced strain localization and failure of austenitic stainless steels at high hydrogen concentrations,” *Acta metallurgica et materialia,* vol. 39, no. 6, pp. 1237-1248, 1991.

[8] M. Whiteman and A. Troiano, *Physica status solidi,* vol. 7, pp. 109-110, 1964.

[9] K. Nibur, B. Somerday, D. Balch and C. San Marchi, “The role of localized deformation in hydrogen-assisted crack propagation in 21Cr-6Ni-9Mn stainless steel,” *Acta materialia,* vol. 57, pp. 3795-3809, 2009.

[10] O. Sobol, G. Nolze, R. Saliwan-Neumann, D. Eliezer, T. Boellinghaus and W. Unger, “Novel approach to image hydrogen distribution and related phase transformation in duplex stainless steel at sub-micron scale,” *international journal of hydrogen energy,* vol. 42, pp. 25114-25120, 2017.

[11] A. Glowacka, M. Wozniak and W. Swiatnicki, “AFM study of austeno-ferritic stainless steel microstructure after cathodic hydrogen charging,” *Journal of alloys and compounds,* Vols. 404-406, pp. 595-598, 2005.

[12] L. Claeys, T. Depover, I. De Graeve and K. Verbeken, “Electrochemical hydrogen charging of duplex stainless steel,” *Corrosion,* p. https://doi.org/10.5006/2959, 2019.

[13] K. Verbeken, N. Van Caenegem and M. Verhaege, “Quantification of the amount of epsilon martensite in a Fe-Mn-Si-Cr-Ni shape memory alloy by means of electron backscatter diffraction,” *Materials science and engineering A,* Vols. 481-482, pp. 471-475, 2008.

[14] K. Verbeken, N. Van Caenegem and D. Raabe, “Identification of epsilon martensite in a Fe-based shape memory alloy by means of EBSD,” *Micron,* vol. 40, pp. 151-156, 2009.

[15] W. Luu, P. Liu and P. Wu, “Hydrogen transport and degradation of a commercial duplex stainless steel,” *Corrosion science,* vol. 44, pp. 1783-1791, 2002.

[16] S. Chen, T. Wu and J. Wu, “Effects of deformation on hydrogen degradation in a duplex stainless steel,” *Journal of materials science,* vol. 39, pp. 67-71, 2004.

[17] S.-L. Chou and W.-T. Tsai, “Effect of grain size on the hydrogen-assisted cracking in duplex stainless steels,” *Materials science and engineering A,* vol. 270, pp. 219-224, 1999.

[18] J. Zelinski and C. San Marchi, “Technical reference on hydrogen compatibility of materials: high alloy ferritic steels: duplex stainless steels,” Sandia national laboratories, Livermore, 2008.

[19] W. Reick, M. Pohl and A. Padilha, “Determination of the stacking fault energy of austenite in a duplex stainless steel,” *Materials technology,* vol. 67, no. 6, pp. 253-256, 1996.

[20] T. Zakroczymski, A. Glowacka and W. Swiatnicki, “Effect of hydrogen concentration on the embrittlement of a duplex stainless steel,” *Corrosion science,* vol. 47, pp. 1403-1414, 2005.

[21] H. Luo, C. Dong, Z. Liu, M. Maha and X. Li, “Characterisation of hydrogen charging of 2205 duplex stainless steel and its correlation with hydrogen-induced cracking,” *Materials and corrosion,* vol. 64, no. 1, pp. 26-33, 2013.

[22] J. Hsu, S. Tsai and H. Shih, “Hydrogen embrittlement of SAF 2205 duplex stainless steel,” *Corrosion,* vol. 58, no. 10, pp. 858-862, 2002.

[23] N. Kheradmand, R. Johnsen, J. Olsen and A. Barnoush, “Effect of hydrogen on the hardness of different phases in super duplex stainless steel,” *International journal of hydrogen energy,* vol. 41, pp. 704-712, 2016.

[24] T. Depover, T. Hajilou, D. Wan, D. Wang, A. Barnoush and K. Verbeken, “Assesment of the potential of hydrogen plasma charging as compared to conventional electrochemical hydrogen charging on dual phase steel,” *Materials science and engineering A,* 2019.

[25] S. Harjo, Y. Tomota and M. Ono, “Measurements of thermal residual elastic strains in ferrite-austenite Fe-Cr-Ni alloys by neutron and X-ray diffractions,” *Acta materialia,* vol. 47, no. 1, pp. 353-362, 1999.

[26] A. Barnoush, M. Zamanzade and H. Vehoff, “Direct observation of hydrogen-enhanced plasticity in super duplex stainless steel by means of in situ electrochemical methods,” *Scripta materialia,* vol. 62, pp. 242-245, 2010.

[27] J. Li, W. Zheng and Q. Jiang, “Stacking fault energy of iron-base shape memory alloys,” *Materials Letters,* vol. 38, pp. 275-277, 1999.

[28] I. Robertson, D. Lillig and P. Ferreira, “Revealing the fundamental processes controlling hydrogen embrittlement,” *Proceedings of the 2008 International hydrogen conference,* pp. 22-37, 2009.

[29] X.-S. Yang, S. Sun and T.-Y. Zhang, “The mechanism of bcc alpha' nucleation in single hcp epsilon laths in the fcc gamma, hcp epsilon to alpha' martensite phase transformation,” *Acta materialia,* vol. 95, pp. 264-273, 2015.

[30] L. Zhang, Z. Li, J. Zheng, Y. Zhao, P. Xu, C. Zhou and X. Li, “Effect of strain-induced martensite on hydrogen embrittlement of austenitic stainless steels investigated by combined tension and hydrogen release methods,” *International journal of hydrogen energy,* vol. 38, no. 19, pp. 8208-8214, 2013.

[31] Y. Kim, N. Kang, Y. Park, I. Choi, G. Kim, S. Kim and K. Cho, “Effects of the strain induced martensite transformation on the delayed fracture of Al-added TWIP steel,” *Journal of the Korean institute of metals and materials,* vol. 46, no. 12, pp. 780-787, 2008.

[32] R. Nishimura and O. Alyousif, “A new aspect on intergranular hydrogen embrittlement of solution annealed types 304,316 and 310 austenitic stainless steels,” *Corrosion Science,* vol. 51, pp. 1894-1900, 2009.

[33] C. San Marchi, K. Nibur, D. Balch, B. Somerday, X. Tang, G. Schiroky and T. Michler, “Hydrogen-assisted fracture of austenitic stainless steels,” in *Effects of hydrogen on materials*, Wyoming, 2009.